J Solid State Electrochem (2005) 9: 154–167
DOI 10.1007/s10008-004-0566-1

ORIGINAL PAPER

I. Betova · M. Bojinov · Tz. Tzvetkoff

Transpassive dissolution mechanism of ferrous alloys in phosphoric acid/acetic acid mixtures

Received: 12 January 2004 / Accepted: 7 May 2004 / Published online: 20 August 2004

Abstract The transpassive dissolution of Fe-12%Cr and Fe-25%Cr alloys in near-anhydrous phosphoric acid/acetic acid mixtures has been studied by conventional voltammetry and electrochemical impedance spectroscopy. Both steady-state and transient techniques point to two parallel pathways for the process involving oxidative dissolution of Cr as Cr(VI) and isovalent dissolution of Fe most probably mediated by an electrolyte-originating species. A simplified kinetic model of the process including only surface kinetic steps has been found to reproduce successfully both the steady-state and the small-amplitude AC response of the studied materials. The kinetic parameters of the model are determined and their relevance regarding the influence of the alloy and electrolyte composition on the relative importance of the two parallel pathways is discussed. The experimental data and model calculations indicate that the effect of acetic acid on the reaction steps related to dissolution of Fe is more significant.

Keywords Iron–chromium alloys · Transpassive dissolution · Surface reactions · Electrochemical impedance spectroscopy · Kinetic model

Abbreviations

b_i	Tafel coefficients of the interfacial reactions (i = 31, 5, 6), V^{-1}
C_d	capacitance of the film–solution interface, F cm^{-2}
Cr_m	chromium atom in the metal phase
Cr^{III}_{Cr}	chromium(III) in a chromium position in the anodic film
Cr^{4+}_{ad}	chromium(IV) intermediate adsorbed at the film–solution interface
Cr^{6+}_{aq}	solvated Cr(VI) ion in the electrolyte
E	applied potential, V
Fe^{III}_{Cr}	iron(III) in a chromium position in the anodic film
Fe^{3+}_{ad}	iron(III) surface complex adsorbed at the film–solution interface
Fe^{3+}_{aq}	solvated iron(III) ion in the electrolyte
Fe_m	iron atom in the metal phase
I	current density, A cm^{-2}
j	imaginary unit
k_i	rate constants of the interfacial reactions (i = 31, 32, 5, 6), mol cm^{-2} s^{-1}
k_i^0	values of the rate constants of the interfacial reactions (i = 31, 32, 5, 6) at the thermodynamic equilibrium potential of the Cr(III)/Cr(VI) couple, mol cm^{-2} s^{-1}
R_t	charge transfer resistance, Ω cm^2
$V_{Cr}^{'''}$	chromium cation vacancy in the anodic film
x_{Fe}	iron(III) position in the anodic film bulk
α	polarizability of the film–solution interface
α_i	transfer coefficients of the interfacial reactions (i = 31, 5, 6)
β	total number of cation positions in the outermost layer of the anodic film, mol cm^{-2}
γ_{Cr}	fraction of chromium(III) positions in the outermost layer of the anodic film
γ_{Fe}	fraction of iron positions in the outermost layer of the anodic film
θ_{Cr}	surface coverage of the chromium(IV) intermediate
θ_{Fe}	surface coverage of the iron(III) intermediate
ω	angular frequency, rad s^{-1}

I. Betova · M. Bojinov (✉)
VTT Technical Research Centre of Finland,
P.O. Box 1704, 02044 VTT, Finland
E-mail: martin.bojinov@vtt.fi
Tel.: +358-9-456-5873
Fax: +358-9-456-5875

T. Tzvetkoff
Department of Physical Chemistry,
University of Chemical Technology and Metallurgy,
1756 Sofia, Bulgaria

Introduction

Electropolishing and surface levelling of steels is used in many industrial applications. In a literature review of the fundamentals of that process [1], it has been

Table 1 Composition of the ferrous alloys used in the present investigation (weight %)

Alloy	Cr	C	Si	Mn	Fe
Fe-12%Cr	11.85	0.015	0.15	0.14	Balance
Fe-25%Cr	24.80	0.015	0.11	0.12	Balance

emphasised that the general aspects of the process are now well understood and can be modelled quantitatively. However, it has also been stated that other aspects such as the properties of anodic electropolishing films and of their interaction with the highly concentrated polishing media need further study [1]. At present, it is not possible to formulate electropolishing electrolytes from theoretical principles. In chemical processing and other industries, common mineral acids such as phosphoric, acetic, formic and perchloric acids frequently come into contact with ferritic steels, but corrosion studies of such steels in concentrated acid mixtures have been scarcely reported [2]. Since these acids and their mixtures are used as polishing electrolytes for different steel-based materials, attention has also been paid to examine the electropolishing behaviour of the alloys in these solutions. The polishing phenomenon is characterized by the disappearance of specific crystallographic or grain-boundary

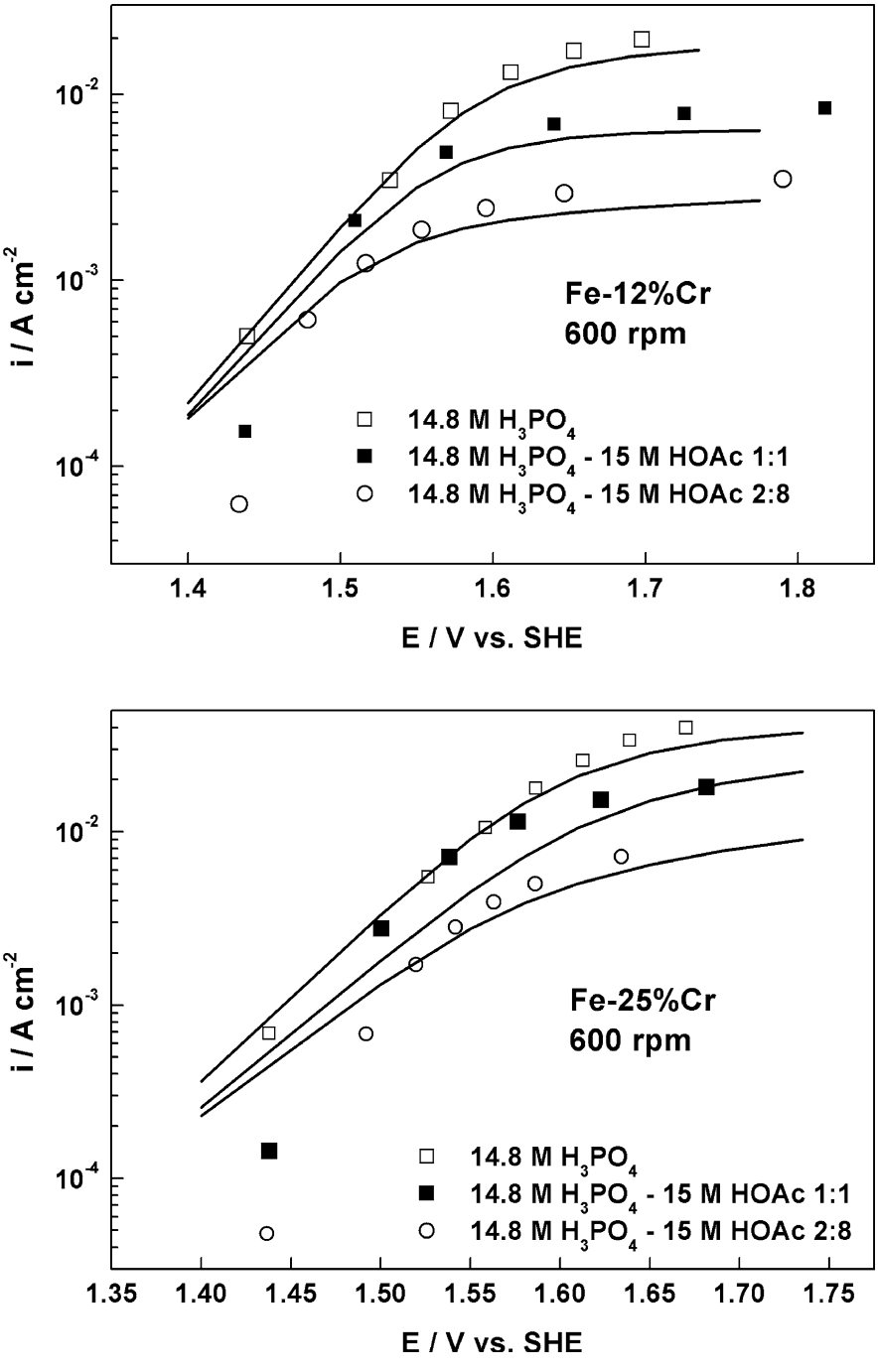

Fig. 1 Steady-state current vs. potential curves in the transpassive state for **a** Fe-12%Cr and **b** Fe-25%Cr in 14.8 M H_3PO_4, 14.8 M H_3PO_4/15 M CH_3COOH (1:1) and 14.8 M H_3PO_4/15 M CH_3COOH (2:8). *Points* experimental values, *solid lines* best-fit calculation according to the kinetic model outlined in the text

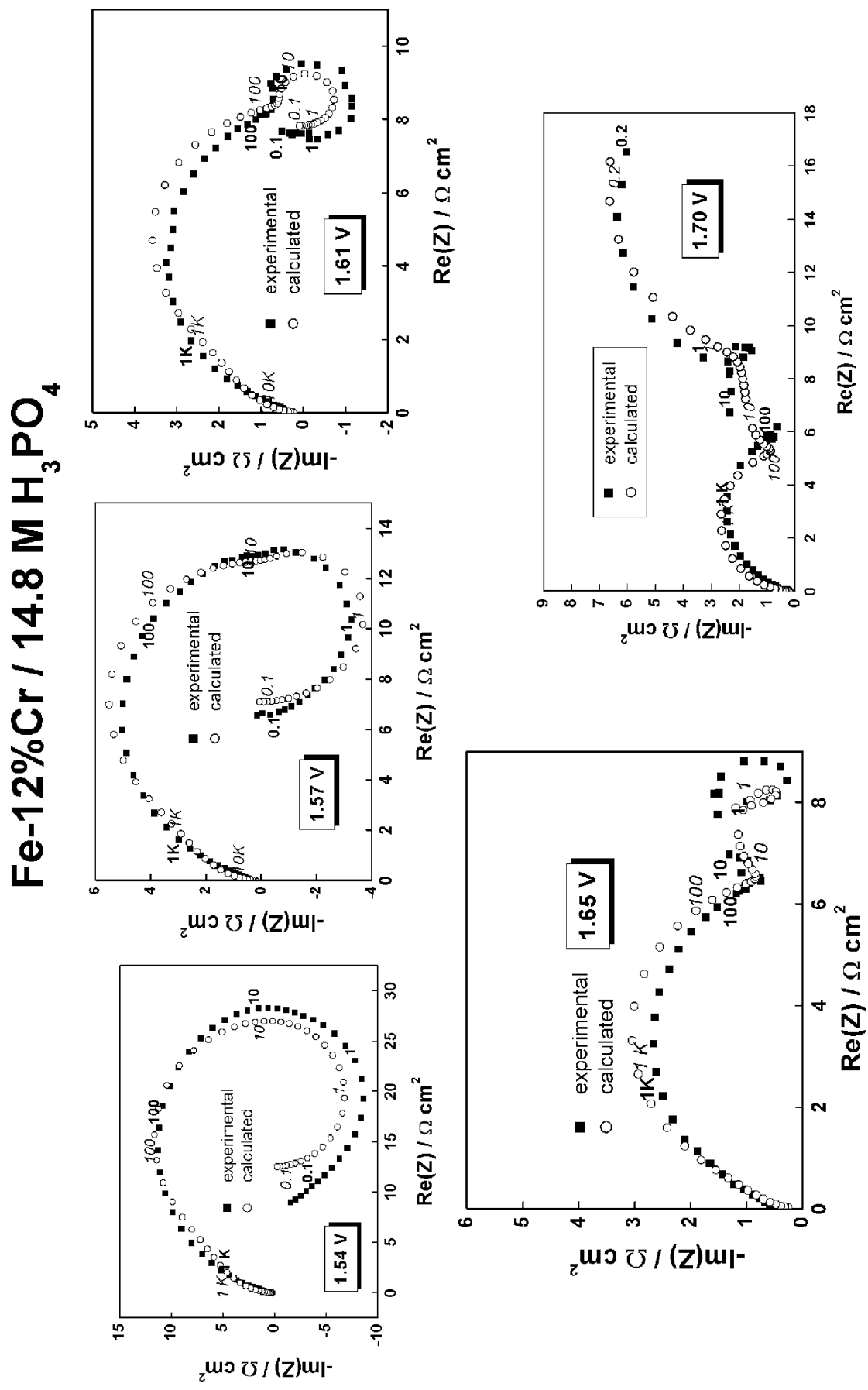

Fig. 2 Impedance spectra measured in the transpassive state of Fe-12%Cr in 14.8 M H_3PO_4. Parameter is frequency in Hz. *Closed symbols* experimental values, *open symbols* best-fit calculation according to the kinetic model outlined in the text

attack on the micron or submicron scale, resulting in a smooth surface with a mirror-like lustre. It has been suggested that the disappearance of oriented dissolution during polishing is caused by a shift of the dissolution mechanism from surface-kinetic control, which may vary from one crystallographic orientation to another, to transport control, which should be insensitive to crystallographic features [1]. It has been proposed that the diffusion-limited process is related to the mass-transport-controlled dissolution of a surface film [1]. However, the mechanism of mass-transport-limited anodic dissolution in phosphoric acid based polishing baths is far less evident and may in fact depend on the nature of the dissolving metal or alloy [3]. Impedance measurements for the iron–chromium system suggested the possibility of a different mechanism for mass-transport-limited polishing in this case, namely, a diffusion limitation for transport of a complexing or solvating acceptor species toward the electrode surface from the bulk electrolyte [4, 5].

In a recent paper, the effect of solution anion on the transpassive dissolution mechanism of model ferritic steels was assessed by comparing the features of the process in 1 M water solutions of H_3PO_4 and H_2SO_4 [6]. It has been demonstrated that the transpassive dissolution rate is lower in H_3PO_4 solution when compared to H_2SO_4, and this fact was tentatively explained by the stabilising effect of the phosphate anion towards the dissolution of Fe through the secondary passive film [6]. In another recent study the accelerating effect of organic acids on the transpassive dissolution rate was explained on the basis of an increase in the rate of iron dissolution by the acid anions acting as complexing agents [7]. As electropolishing of steels is usually carried out in concentrated acid mixtures containing small amounts of water, it is of considerable interest to investigate the effect of organic additives on the transpassive dissolution rate, particularly because successful electropolishing of ferritic steels has already been reported in some of these mixtures in near-room-temperature conditions [2].

The present study discloses the mechanism of transpassive dissolution of Fe–Cr alloys (12% and 25 wt.% Cr) in acetic acid mixtures (14.8 M H_3PO_4/15 M CH_3COOH 1:1 and 2:8). Experimental data obtained by using voltammetric and impedance spectroscopic measurements with rotating disc electrodes are presented and discussed. A simplified kinetic model is then proposed to explain the experimental results, and the values of kinetic parameters are estimated and discussed in relation to their relevance to electropolishing.

Experimental

Electrodes and electrolytes

Laboratory-made Fe-12%Cr and Fe-25%Cr alloys were used as working electrode materials. Their compositions determined by atomic absorption spectrometry are given in Table 1. For the voltammetric and electrochemical impedance spectroscopic measurements, cylindrical pieces machined off the studied materials were embedded in Kel-F holders to produce rotating disc electrodes (exposed area 0.16 cm^2). The working electrode pretreatment consisted of mechanical polishing on emery paper up to 4,000 grade, degreasing and rinsing with water purified in a Milli-Q water purification system. A three-electrode cell featuring a Pt counter electrode and a saturated calomel reference electrode was employed. All the potentials in the paper are converted to the standard hydrogen electrode (SHE) scale. Electrolyte mixtures have been prepared from reagent grade 14.8 M H_3PO_4 (85%) and 15 M CH_3COOH (90%). The experiments were carried out at 20 ± 1°C in solutions deaerated with pure nitrogen (99.999%).

Apparatus and procedures

Voltammetric and impedance spectroscopic measurements were carried out with an Autolab PGSTAT 30 potentiostat/galvanostat equipped with a frequency response analyser module and driven by GPES 4.9 and FRA software (Eco Chemie, The Netherlands). A rotating disc electrode setup has been employed in the range of rotation rates 300–1,800 rpm. At each polarisation potential, the current vs. time curve was recorded until a steady state was reached (according to the criterion that current variation is less than 2%). All the potential values were corrected for the IR drop determined by the product of the steady-state current and the high-frequency intercept of the impedance spectra. The impedance spectra were measured at this steady state in the frequency range 0.02–11,000 Hz at an AC amplitude of 10 mV (rms). The reproducibility of the impedance spectra was $\pm 1\%$ by magnitude and $\pm 2°$ by phase angle. The linearity condition was verified by measuring spectra at amplitudes ranging between 2 and 20 mV (rms). The causality was checked by a Kramers–Kronig test included in the FRA 4.9 software, and the points that did not pass the test (usually at the low-frequency end) were discarded. The fitting of the impedance spectra to the transfer function derived on the basis of a kinetic model was performed by using Microcal Origin 6.0 software. Statistical weighting was used for the experimental data set, and the errors of parameter estimation were multiplied by the square root of the reduced chi-square value resulting from the fit. The standard error of estimate of the kinetic parameters calculated by the procedure did not exceed $\pm 5\%$.

Results

Voltammetric measurements

Figure 1 summarizes the steady-state polarisation curves of the Fe-12%Cr (Fig. 1a) and Fe-25%Cr alloys (Fig. 1b)

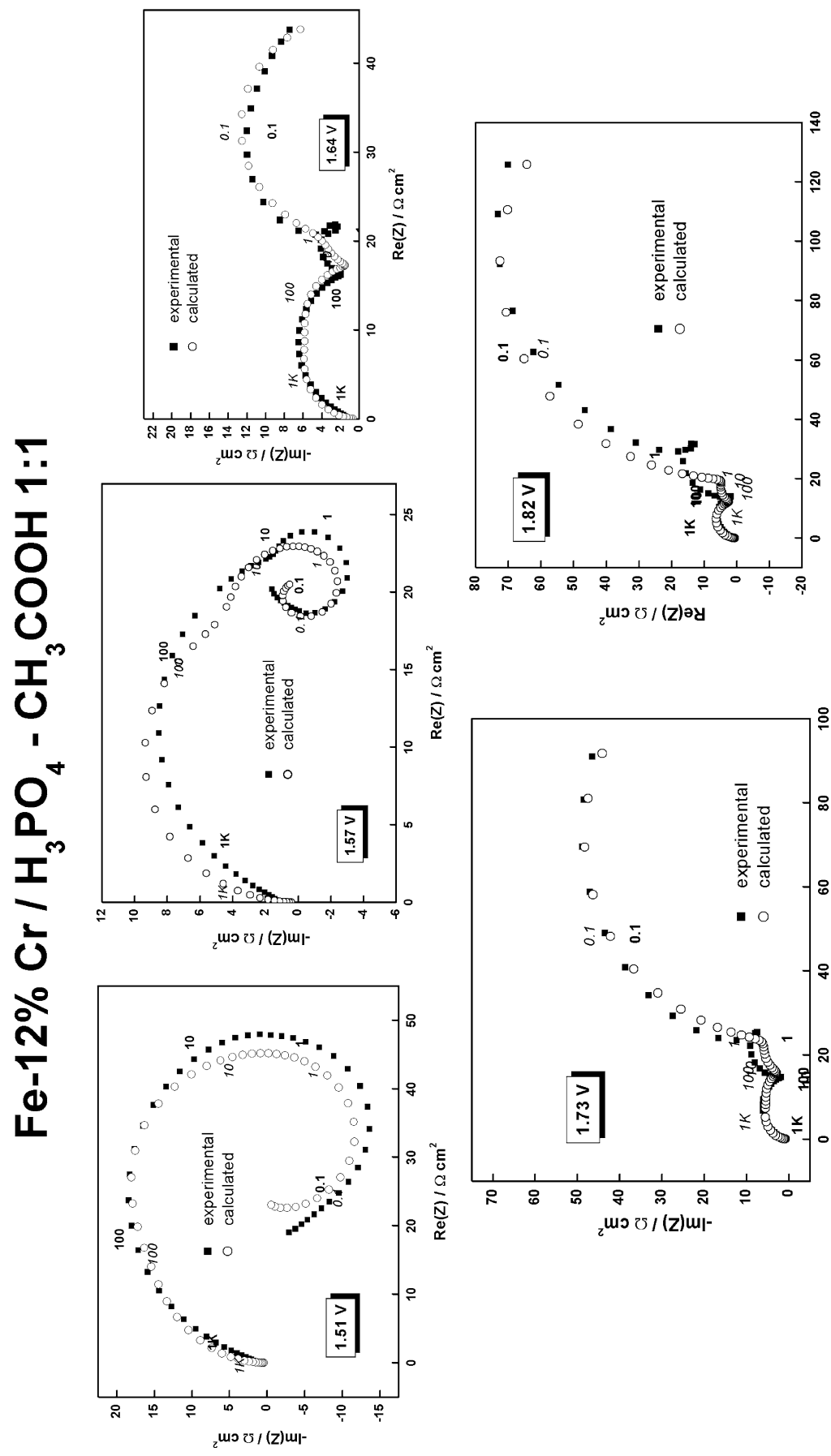

Fig. 3 Impedance spectra measured in the transpassive state of Fe-12%Cr in 14.8 M H_3PO_4/15 M CH_3COOH (1:1). Parameter is frequency in Hz. *Closed symbols* experimental values, *open symbols* best-fit calculation according to the kinetic model outlined in the text

in 14.8 M H_3PO_4 and in binary mixtures of 14.8 M H_3PO_4/15 M CH_3COOH (1:1) and 14.8 M H_3PO_4/15 M CH_3COOH (2:8), measured in the transpassive region with a rotating disc electrode (rotation rate 600 rpm). It is worth mentioning that the effect of electrode rotation (300–1800 rpm) on both the shape of the curves and the current magnitude is small, in analogy to the measurements in 1 M aqueous solutions of H_3PO_4 and H_2SO_4 [6]. This most probably indicates that the role of bulk solution transport in the overall dissolution process is negligible.

All curves comprise two Tafel-like regions, separated by an inflection point at approximately 1.55 V, and a quasi-plateau region at the high-potential end. This fact indicates that the dissolution mechanism is similar in concentrated phosphoric acid electrolyte and in the mixtures with different acetic acid contents. A comparison of the curves for both alloys in 14.8 M H_3PO_4 with those in the 1:1 and 2:8 mixtures indicates that in the first Tafel-like region, the currents are very similar, regardless of the alloy or solution composition (Fig. 1). Such a finding is in agreement with our previous results in 1 M solutions of H_3PO_4 or H_2SO_4 [6]. Conversely, the currents in the potential range 1.55–1.75 V are smaller, the higher the content of acetic acid (Fig. 1). Moreover, the quasi-plateau currents for the Fe-25%Cr alloy are almost half an order of magnitude greater than that on Fe-12%Cr, which is obviously related to the higher Cr content of the former alloy. In summary, the effect of acetic acid addition on the curves is analogous to that reported in ref. [2] and is more of a quantitative nature (i.e. the overall mechanism of the process is not affected). Rather, acetic acid has a clear decelerating influence on the rate-limiting step of the transpassive dissolution in the second Tafel-like region and the quasi-plateau region.

Electrochemical impedance spectroscopic measurements

In order to identify the number of reaction steps that are detectable by electrochemical means and to assess in a more quantitative fashion the effect of acetic acid on these steps, impedance measurements were performed in the transpassive dissolution range. Figures 2, 3 and 4 summarise the results obtained for the Fe-12%Cr alloy in 14.8 M H_3PO_4 and the two mixtures (1:1 and 2:8), whereas the corresponding results for the Fe-25%Cr alloy are collected in Figs. 5, 6 and 7. It is worth mentioning that the uncompensated electrolyte resistances have been subtracted from all the spectra in order to enable a better comparison between data in different mixtures (the conductivity of the acetic acid containing electrolytes, especially the 2:8 mixture, is considerably lower than that of the 14.8 M H_3PO_4).

In the first Tafel-like region (below 1.55 V), the impedance spectra exhibit the characteristic shape pertinent to the transpassive dissolution of Cr and Fe–Cr alloys in a range of media [3, 6, 7, 8, 9, 10]. That is, they comprise a high-frequency capacitive loop usually ascribed to the parallel combination of an interfacial capacitance and charge-transfer resistance, and a low-frequency pseudo-inductive loop related to the relaxation of the surface coverage of an intermediate accelerating the reaction rate in the transient regime [6, 8, 9, 10]. The fact that pseudo-inductive behaviour is observed in a relatively large potential domain indicates that there are at least two intermediate states in the overall dissolution process [11]. In the potential region below 1.55 V, both the shape of the spectra and the magnitude of the impedance at low frequencies (interpreted as the polarisation resistance) are only slightly dependent on the alloy and solution composition (Figs. 2, 3, 4, 5, 6 and 7). This fact is in accordance with the voltammetric results depicted in Fig. 1. It most probably means that the main process in this region is similar regardless of the variety of the conditions explored in the present work and can be identified with the transpassive dissolution of Cr from the alloy [6, 8, 9, 10].

At potentials higher than 1.55 V, two further capacitive loops can be gradually discerned in the impedance spectra for the two materials in all the investigated media (Figs. 2, 3, 4, 5, 6 and 7). In general, capacitive loops can be ascribed to the relaxation of surface coverages of intermediate species decelerating the overall reaction rate in the transient regime [6]. In other words, the accumulation of that kind of species at the interface would promote secondary passivation. The first capacitive loop is detected as a hump at approximately 10 Hz and its size relative to the highest-frequency loop seems to grow as the potential is increased. The second loop gradually manifests itself at the low-frequency end and becomes the dominant feature of the spectra for Fe-12%Cr at the highest potentials, especially in the 2:8 mixture (cf. Figs. 3 and 4). For Fe-12%Cr, the inductive loop gradually disappears with increasing potential, being masked by the low-frequency capacitive feature. This can be interpreted as secondary passivation reactions gradually taking over transpassive dissolution as the potential is increased. Such an evolution of the spectra for Fe-12%Cr is most pronounced in the 2:8 electrolyte mixture, indicating that acetic acid addition seems to favour the secondary passivation reactions, which correlates well with the lowest current densities and the highest polarisation resistance values in the plateau region for this particular mixture (Fig. 1a and Fig. 4). It is worth noticing that such a change in behaviour cannot be explained on the basis of the lowering of the concentration of phosphoric acid alone, because impedance spectra for Fe-12%Cr in 1 M H_3PO_4 show a different evolution with potential [6].

Regarding the effect of Cr content, the present results show that the lowest-frequency capacitive loop is almost undetectable for Fe-25%Cr in 14.8 M H_3PO_4 (Fig. 5) and its size remains small relative to the capacitive loop at approximately 10 Hz for the same material in the 1:1

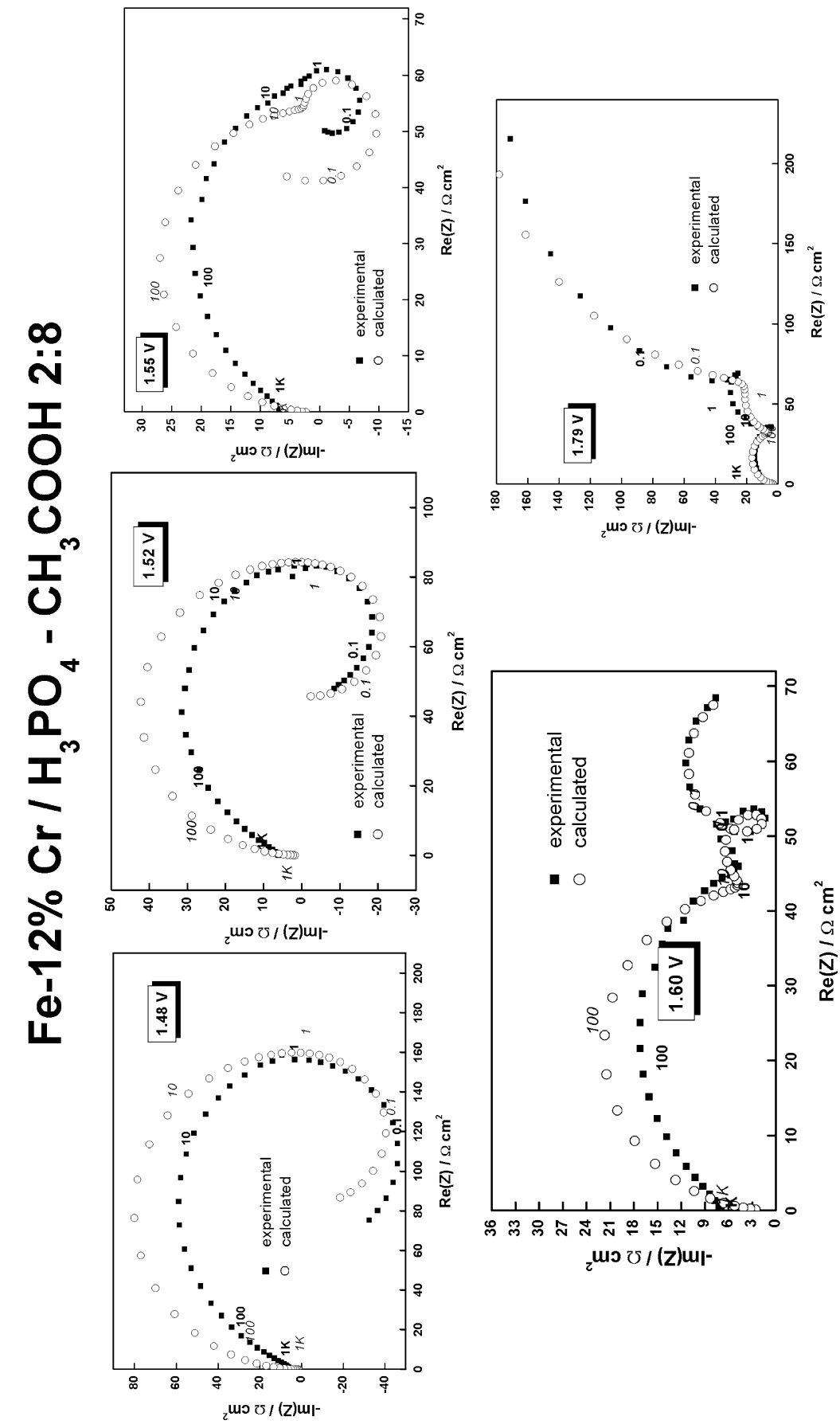

Fig. 4 Impedance spectra measured in the transpassive state of Fe-12%Cr in 14.8 M H_3PO_4/15 M CH_3COOH (2:8). Parameter is frequency in Hz. *Closed symbols* experimental values, *open symbols* best-fit calculation according to the kinetic model outlined in the text

and 2:8 mixtures (Figs. 6 and 7). This most probably means that the distribution of the intermediate species at the interface is different for the Fe-25%Cr alloy in comparison to Fe-12%Cr. Such a suggestion is supported by the fact that the pseudo-inductive behaviour is prominent in the whole potential range for Fe-25%Cr in the 14.8 M H_3PO_4 (Fig. 5). However, in the 1:1 and 2:8 mixtures it also gets gradually masked by capacitive behaviour at the highest studied potentials (Figs. 6 and 7). This means that acetic acid favours the secondary passivation process for the Cr-rich alloy as well.

In summary, the impedance data point to the existence of at least three intermediate species in the transpassive dissolution reaction, one of them accelerating the overall reaction rate in the transient regime and the remaining two decelerating that rate (i.e. leading to some sort of secondary passivation). The addition of acetic acid seems to favour the reaction steps related to the accumulation of the intermediates related to secondary passivation. This tendency is significantly stronger for the alloy containing less Cr (i.e. it is tempting to associate the action of acetic acid with its effect on the interfacial reaction steps involving the main element, Fe).

Discussion

Reaction model—main assumptions and simplifications

A successful physical model of the alloy–electrolyte system during transpassive dissolution of ferrous alloys in H_3PO_4/CH_3COOH mixtures has to be able to explain the following experimental features:

- the existence of two parallel reaction paths in the transpassive dissolution process as evidenced both by the steady-state polarisation curves and the impedance measurements;
- the appearance of at least two time constants in the impedance spectra below about 1.55 V, as well as the two extra capacitive loops observed at higher potentials;
- the effect of acetic acid on transpassive dissolution being the most pronounced in the second Tafel-like potential range and the quasi-plateau region (i.e. most probably related to the deceleration of the reactions involving the dissolution of Fe species).

The kinetic model presented in this section to meet these criteria is built up using the so-called acceptor model for electropolishing of ferritic steels advanced in a series of papers by Matlosz et al. [3, 4, 5] and the generalised model for transpassive dissolution discussed at length in our previous paper [6] as a basis. As a full-scale superposition of the two models would have certainly resulted in a quasi-intractable set of equations, several simplifications are introduced. The main assumptions of the model are listed below.

In accordance with both our previous paper [6] and the work by Matlosz et al. [3, 4, 5], the processes taking place in the transpassive region are considered to be limited by reaction steps taking place at the oxide film–solution interface and resulting in the generation of cation vacancies.

The transport of cation vacancies through the oxide is assumed to proceed via high-field assisted migration whose rate is proposed to be adjusted by the rates of the interfacial reactions that generate cation vacancies.

The growth of the oxide in the transpassive region is neglected as a slow reaction in parallel to transpassive dissolution for the sake of simplicity. Indeed, current efficiencies close to 100% for the transpassive dissolution have been reported [12], supporting such a simplification.

The applied potential is distributed between the film–solution interface and the oxide film itself [6]. In other words, a fraction αE of the applied potential is consumed as a potential drop at the film–solution interface where α is the polarisability of that interface [13].

The potential drop at the inner interface is assumed to be small and independent on the applied potential [6]. This means that the reactions at the metal–film interface are not rate limiting. Their rates are adjusted by the rates of point defect transport.

No transport limitations for any species in the bulk electrolyte are taken into account by the model. This assumption is at variance to the treatment of Matlosz et al. [4, 5] in which a transport step of the complexing/solvating agent in the bulk of the electrolyte has been included. However, as the effect of the rotation rate of the electrode on both the current vs. potential curves and impedance spectra measured in the present work has been found to be small, neglecting such a transport step is believed to be consistent with experiment.

Reaction steps considered in the model

The following set of reactions is proposed to occur at the film–solution interface and limit the rate of the overall process in the transpassive dissolution region:

$$\begin{aligned}
&Fe^{III}_{Cr}(\gamma_{Fe}) \xrightarrow{k_{31}} Fe^{3+}_{ad}(\theta_{Fe}) + V'''_{Cr}\\
&Fe^{3+}_{ad}(\theta_{Fe}) \xrightarrow{k_{32}} Fe^{3+}_{aq}\\
&Cr^{III}_{Cr}(\gamma_{Cr}) \xrightarrow{k_5} Cr^{4+}_{ad}(\theta_{Cr}) + e' + V'''_{Cr}\\
&Cr^{4+}_{ad}(\theta_{Cr}) \xrightarrow{k_6} Cr^{6+}_{aq} + 2e'
\end{aligned} \qquad (1)$$

The k_{31}–k_{32} reaction sequence is in principle analogous to that proposed by Matlosz et al. [4, 5]. In that sense, the k_{31} step is associated with the ion transfer from the cation sublattice to an adsorbed state, possibly involving a surface complexation step with an anion or a water-originating species from the electro-

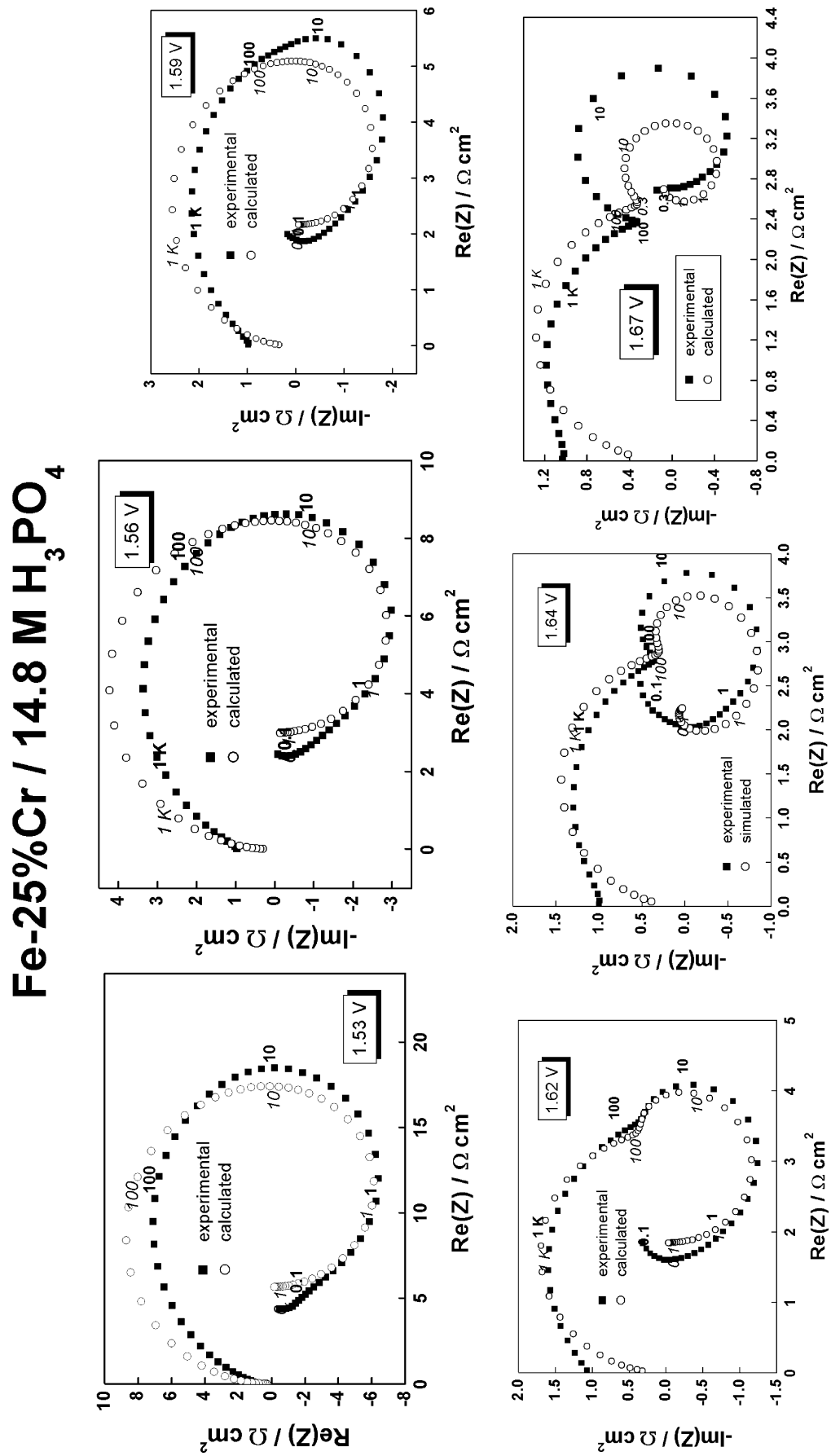

Fig. 5 Impedance spectra measured in the transpassive state of Fe-25%Cr in 14.8 M H_3PO_4. Parameter is frequency in Hz. *Closed symbols* experimental values, *open symbols* best-fit calculation according to the kinetic model outlined in the text

lyte. The k_{32} step is the desorption of the $Fe^{3+}{}_{ad}$ species into the electrolyte, possibly featuring another surface complexation step. As only electrochemical methods are used in the present study, the chemistry of these surface complexation reactions is not introduced in any detail and a skeletal representation is preferred. The k_5–k_6 sequence is the usual two-step process of transpassive dissolution of Cr, discussed at length in our previous paper [6]. The cation vacancies generated by both reactions of formation of adsorbed intermediates are transported through the oxide via high-field assisted migration and are consumed at the metal–film interface via the following set of reactions:

$$\begin{aligned} Cr_m + V'''_{Cr} &\xrightarrow{k_{11}} Cr^{III}_{Cr} + 3e' \\ Fe_m + V'''_{Cr} &\xrightarrow{k_{12}} Fe^{III}_{Cr} + 3e' \end{aligned} \tag{2}$$

However, as discussed above, neither the transport nor the reactions at the metal–film interface are considered to be rate limiting. This means that we intend to describe the behaviour of the system solely in terms of the reaction sequence (1). Since this sequence comprises two parallel reaction paths and three independent surface positions or coverages with adsorbed species, it qualitatively fulfils the requirements set in the beginning of the ''Discussion'' section by the obtained experimental data.

Reaction model—main equations

Charge and material balances

In writing the charge and mass balances, we implicitly assume that the oxide on the steel in the transpassive region is based on Cr_2O_3 with some Fe(III) (mass fraction x_{Fe}) substituting for Cr. It is also assumed that all changes in composition due to transpassive dissolution of Cr are restricted to the outermost cation layer of the oxide, β being the total concentration of available cation sites. In the outermost layer, the corresponding Cr- and Fe-positions are labelled γ_{Cr} and γ_{Fe}, and the apparent coverages of the $Fe^{3+}{}_{ad}$ and $Cr^{4+}{}_{ad}$ intermediates are θ_{Fe} and θ_{Cr}. The reaction steps k_{31}, k_5 and k_6 are considered to be electrochemical, that is, their rate constants depend exponentially on the potential drop at the film–solution interface: $k_i = k^0{}_i \exp(b_i \alpha E)$, i = 31, 5, 6, where $k^0{}_i$ are the values of the rate constants at the thermodynamic equilibrium potential of the Cr(VI)/Cr(III) couple and $b_i = \alpha_i n_i F/RT$, where α_i is a transfer coefficient and n_i the number of transferred electrons. Conversely, the complexation/desorption step k_{32} is considered to be a chemical reaction in accordance with the treatment of Matlosz et al. [4], that is, its rate is independent of the applied potential.

In view of these assumptions, the charge and mass balances are given by the following equations:

$$\begin{aligned} I &= F(3k_{31}\gamma_{Fe} + k_5\gamma_{Cr} + 2k_6\theta_{Cr}) \\ \beta\frac{d\gamma_{Fe}}{dt} &= k_6\theta_{Cr}x_{Fe} - k_{31}\gamma_{Fe} + k_{32}\theta_{Fe}x_{Fe} \\ \beta\frac{d\gamma_{Cr}}{dt} &= k_6\theta_{Cr}x_{Cr} + k_{32}\theta_{Fe}x_{Cr} - k_5\gamma_{Cr} \\ \beta\frac{d\theta_{Cr}}{dt} &= k_5\gamma_{Cr} - k_6\theta_{Cr} \\ \beta\frac{d\theta_{Fe}}{dt} &= k_{31}\gamma_{Fe} - k_{32}\theta_{Fe} \\ \frac{d\gamma_{Cr}}{dt} + \frac{d\gamma_{Fe}}{dt} + \frac{d\theta_{Cr}}{dt} + \frac{d\theta_{Fe}}{dt} &= 0 \end{aligned} \tag{3}$$

Steady-state solution

The steady-state solution is obtained by setting the above time derivatives to zero

$$\bar{I} = 3F\left(k_{31}\bar{\gamma}_{Fe} + k_6\bar{\theta}_{Cr}\right) \tag{4}$$

where

$$\begin{aligned} \bar{\theta}_{Cr} &= \frac{k_{31}k_{32}k_5(1-x_{Fe})}{(k_{31}+k_{32})k_5k_6x_{Fe} + k_{31}k_{32}(k_5+k_6)(1-x_{Fe})} \\ \bar{\theta}_{Fe} &= \frac{k_{31}k_5k_6x_{Fe}}{(k_{31}+k_{32})k_5k_6x_{Fe} + k_{31}k_{32}(k_5+k_6)(1-x_{Fe})} \\ \bar{\gamma}_{Cr} &= \frac{k_{31}k_{32}k_6(1-x_{Fe})}{(k_{31}+k_{32})k_5k_6x_{Fe} + k_{31}k_{32}(k_5+k_6)(1-x_{Fe})} \\ \bar{\gamma}_{Fe} &= \frac{k_{32}k_5k_6x_{Fe}}{(k_{31}+k_{32})k_5k_6x_{Fe} + k_{31}k_{32}(k_5+k_6)(1-x_{Fe})} \\ \bar{\gamma}_{Cr} + \bar{\gamma}_{Fe} + \bar{\theta}_{Cr} + \bar{\theta}_{Fe} &= 1 \end{aligned} \tag{a}$$

Small-amplitude AC solution

The small-amplitude AC solution is obtained by a Taylor expansion of the set of equations (3) around a steady state. The solution of the system of resulting equations gives the following expression for the interfacial impedance of the system:

$$\begin{aligned} Z^{-1} &= R_t^{-1} \\ &\quad + F\frac{[3k_{31}(A_1+jA_2) + k_5(A_3+jA_4) + 2k_5(A_5+jA_6)]}{A_7+jA_8} \\ &\quad + j\omega C_d \end{aligned} \tag{5}$$

where

$$\begin{aligned} R_t^{-1} &= F\left[3b_{31}k_{31}\bar{\gamma}_{Fe} + (b_5+2b_6)\bar{\theta}_{Cr}\right] \\ A_1 &= -\omega\beta[(k_{32}+k_5+k_6)X_1 + x_{Fe}(k_{32}X_3 + k_6X_2)] \\ A_2 &= X_1\left[(k_5+k_6)k_{32} - \omega^2\beta^2\right] \\ &\quad + x_{Fe}\{k_{32}X_2k_6 + [(k_5+k_6)k_{32} - k_5k_6]X_3\} \end{aligned} \tag{b}$$

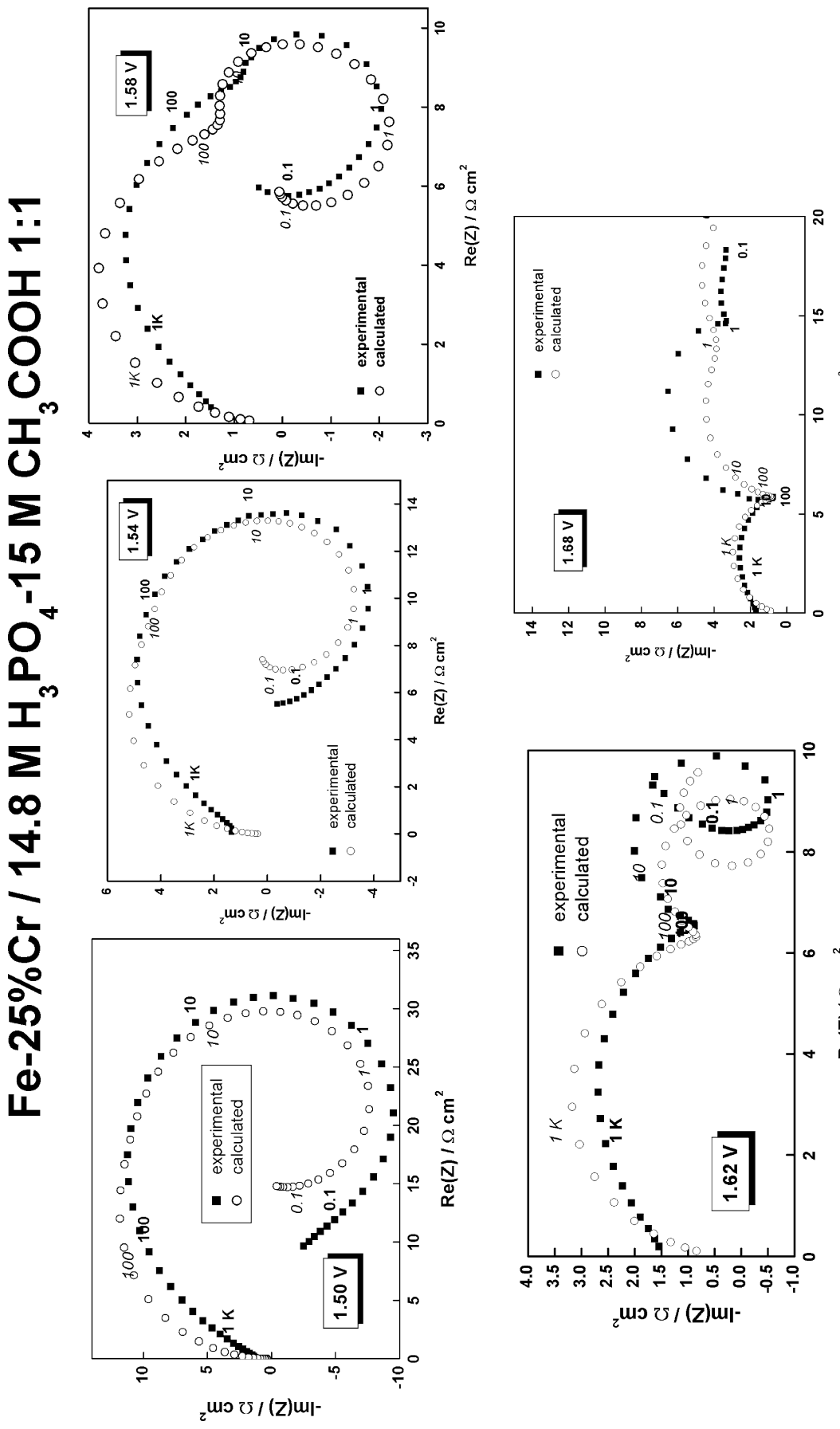

Fig. 6 Impedance spectra measured in the transpassive state of Fe-25%Cr in 14.8 M H_3PO_4/15 M CH_3COOH (1:1). Parameter is frequency in Hz. *Closed symbols* experimental values, *open symbols* best-fit calculation according to the kinetic model outlined in the text

$$A_3 = \omega\beta\left[(k_{31}+k_{32}+k_6)X_1 + (k_{31}+k_{32}+k_6x_{Fe})X_2 + (k_{31}+k_{32}x_{Fe}+k_6)X_3\right]$$
$$A_4 = (X_1+X_2+X_3)\omega^2\beta^2 - (k_{31}+k_{32})k_6X_1 - (k_{31}+k_{32}x_{Fe})k_6X_3 - \left\{\left[(1-x_{Fe})k_{32}+k_6x_{Fe}\right]k_{31} - k_{32}k_6x_{Fe}\right\}X_2 \quad (c)$$

$$A_5 = \omega\beta\left[(X_1+X_3)k_5 - X_2(k_{31}+k_{32})\right]$$
$$A_6 = (1-x_{Fe})k_{31}k_{32}X_2 - k_5X_1(k_{31}+k_{32}) - k_5X_3(k_{31}+k_{32}x_{Fe}) - \omega^2\beta^2X_2 \quad (d)$$

$$A_7 = \omega^3\beta^3 - \left\{\left[(1-x_{Fe})k_{32}+k_5+k_6\right]k_{31} + (k_5+k_6)k_{32} + k_5k_6x_{Fe}\right\}\omega\beta$$
$$A_8 = \left[(1-x_{Fe})(k_5+k_6)k_{32} + k_5k_6x_{Fe}\right]k_{31} + k_{32}k_5k_6x_{Fe} - (k_{31}+k_{32}+k_5+k_6)\omega^2\beta^2 \quad (e)$$

$$X_1 = b_6k_6\bar{\theta}_{Cr}x_{Fe} - b_{31}k_{31}\bar{\gamma}_{Fe}$$
$$X_2 = (b_5-b_6)\bar{\theta}_{Cr} \quad (f)$$
$$X_3 = b_{31}k_{31}\bar{\gamma}_{Fe}$$

and C_d is the double-layer capacitance at the film–solution interface. In summary, we intend to describe the steady-state and small-amplitude AC response of the system in the transpassive dissolution region with the following set of parameters: $k^0{}_{31}$, k_{32}, $k^0{}_5$, $k^0{}_6$, b_{31}, b_5, b_6, α, β, and x_{Fe}.

Comparison of the model to the experimental data

The expression (5) for the interfacial impedance was split analytically into real and imaginary parts by using Maple 6.1 software. The output functions together with the steady-state current vs. potential expression [Eq. (4)] were simultaneously fitted to the real and imaginary part of the measured impedance for a specific alloy at several polarisation potentials and to the corresponding experimental current vs. potential curve. This procedure resulted in a sufficient number of degrees of freedom in the system to obtain statistically reliable values of the kinetic constants.

The calculated steady-state current vs. potential curves for the studied materials are presented in Fig. 1 (as solid lines), whereas the calculated impedance spectra are shown in Figs. 2, 3, 4, 5, 6 and 7 (as open symbols). The agreement between the experimental and calculated current vs. potential curves for Fe-12%Cr (Fig. 1a) is very good, whereas that for Fe-25%Cr leaves something to be desired (Fig. 1b). The discrepancy between calculated and measured current values in the potential range 1.40–1.50 V is most probably due to the fact that the proposed model neglects the reverse steps of the reactions of transpassive dissolution of Cr (see also refs. [8, 9, 10]). In addition, it can be stated that the small-amplitude AC responses are predicted with sufficient accuracy by the model, even if the exact size of all loops for the spectra at some potentials is not matched. This is the price to be paid for using a global fit of all the impedance data for a particular alloy/electrolyte combination. The main discrepancy lies in the high-frequency end of the spectra and is due to the use of an ideal capacitance instead of a constant-phase element (CPE) in the spectra. Although some very recent treatments pointed to the possibility of explaining the apparent CPE behaviour by a distribution of electrolyte conductivity at corroding interfaces by using an array of cylindrical pores [14] or the presence of exponential defect concentration gradients in steady-state passive films [15], we have preferred not to include such a treatment in our model at this stage.

The calculated values of the kinetic parameters are collected in Table 2. It is worth mentioning that the fraction of iron in the passive film, x_{Fe}, has been kept constant in the calculations for the sake of simplicity. Its value of 0.35 corresponds roughly to the iron content of a typical passive film on ferritic steels in an acidic medium. The values of the double-layer capacitance at the film–solution interface (not shown) have been found to be somewhat potential dependent, preserving a reasonable value of approximately 40–60 μF cm^{-2}. The following main points can be emphasised from a survey of Table 2:

- It is encouraging that the whole set of data (two alloys is three electrolyte mixtures) is reproduced using a rather homogeneous set of kinetic parameters, which is especially true for the kinetic constants characterising the dissolution of Cr from the alloys. This means that the predictions of the model are consistent and can be used for an analysis of the effect of alloy and electrolyte composition on the features of the overall process that are detectable by electrochemical means.
- The rate constant $k^0{}_5$ and the exponential coefficients b_5 and b_6 do not change significantly with either the alloy or the electrolyte composition. This means that the mechanism of transpassive dissolution of Cr is almost similar for all the materials and electrolyte compositions.
- Conversely, the rate constant of the Cr dissolution reaction as chromate ($k^0{}_6$) increases with the increase in Cr content in the alloy and decreases with increasing acetic acid content in the electrolyte mixture. This may point to a different composition and/or structure of the product of this reaction (denoted in general as $Cr^{6+}{}_{aq}$) in different electrolytes. The formation of complex heteroanions containing Cr(VI) could be envisaged, but more data are needed to reach a definite conclusion on the effect of electrolyte composition on the chromate formation reaction.
- The rate constants of both steps of the iron dissolution process in general increase with increasing Cr content in the alloy, which is consistent with the suggestions of Heusler [16] that the rate constant of iron dissolution through passive films in binary Fe–Cr alloys increases with increasing Cr content in the substrate. On the other hand, both $k^0{}_{31}$ and k_{32} decrease significantly with increasing the content of

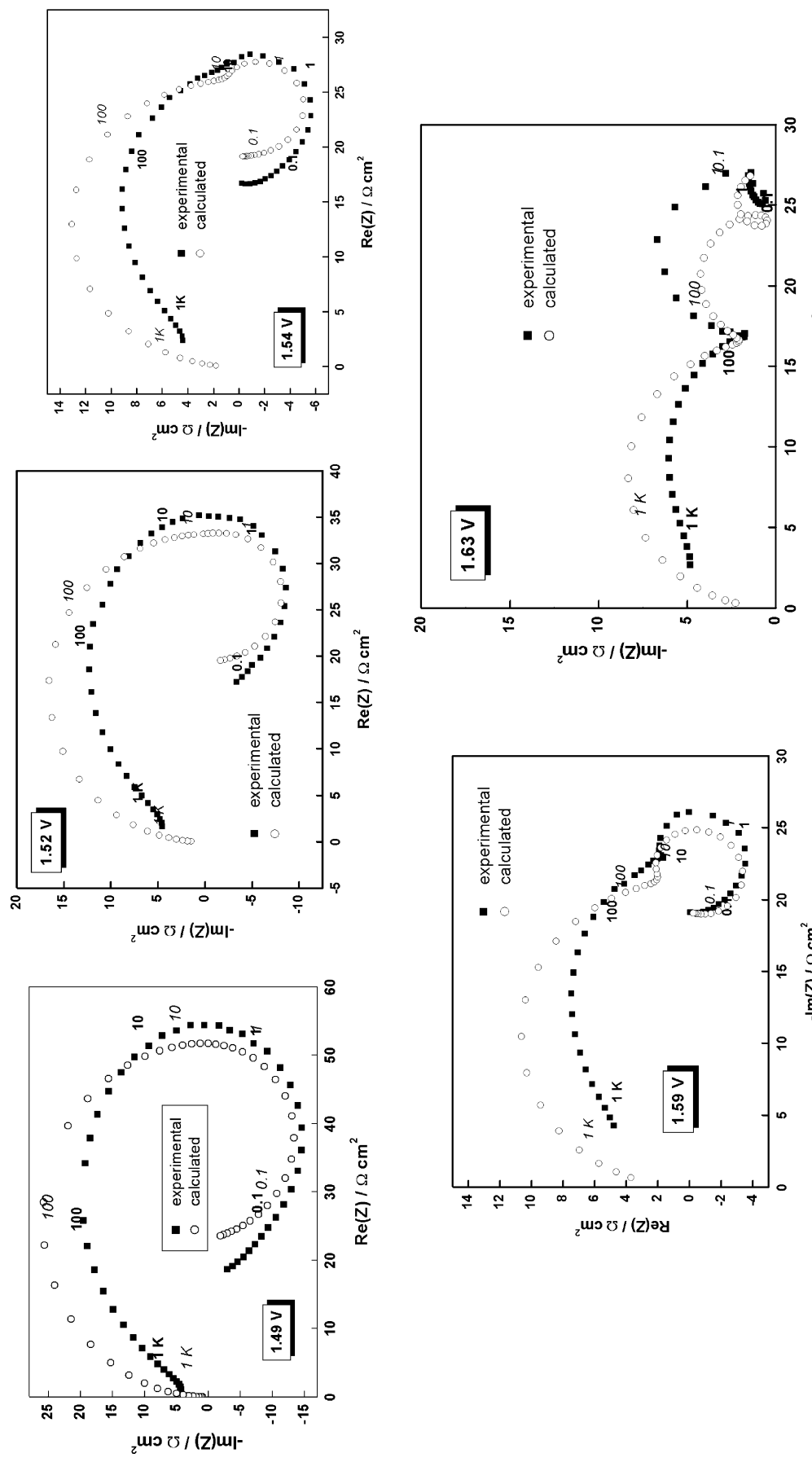

Fig. 7 Impedance spectra measured in the transpassive state of Fe-25%Cr in 14.8 M H_3PO_4/15 M CH_3COOH (2:8). Parameter is frequency in Hz. *Closed symbols* experimental values, *open symbols* best-fit calculation according to the kinetic model outlined in the text

Table 2 Kinetic parameters of the proposed reaction model calculated from the fitting of the model equations to the experimental current vs. potential and impedance data for the studied material/electrolyte combinations

Alloy	Fe-12%Cr			Fe-25%Cr		
14.8 M H_3PO_4/15 M CH_3COOH	1:0	1:1	2:8	1:0	1:1	2:8
$10^8 \times k_{31}{}^0$ (mol cm^{-2} s^{-1})	0.19	0.16	0.15	6.0	3.0	0.61
$10^8 \times k_{32}{}^0$ (mol cm^{-2} s^{-1})	3.1	1.1	0.4	21	3.4	3.4
$10^{12} \times k_5{}^0$ (mol cm^{-2} s^{-1})	2.0	2.5	2.2	5.7	5.5	4.0
$10^8 \times k_6{}^0$ (mol cm^{-2} s^{-1})	1.7	2.4	0.44	5.3	1.5	0.73
$b_{31}(V^{-1})$	22	25	16	14	18	15
$b_5(V^{-1})$	39	38	36	38	38	38
$b_6(V^{-1})$	5.5	5.8	5.0	5.1	6.3	5.2
$10^8 \times \beta$(mol cm^{-2})	2.0	2.0	1.3	3.3	3.5	1.3
α	0.59	0.60	0.61	0.59	0.59	0.6
xFe	0.35	0.35	0.35	0.35	0.35	0.35

acetic acid in the electrolyte mixture, the decrease being more pronounced for the Fe-25%Cr alloy (Table 2). Thus the calculations based on the proposed model are in agreement with the general suggestion made in the ''Experimental'' section that the effect of acetic acid concerns mainly the reactions in the secondary passivation region in which iron species are presumably involved.

– The total number of available cation positions in the outermost layer, β, is considerably smaller in the electrolyte mixture containing mainly acetic acid (H_3PO_4/CH_3COOH 2:8) when compared to the remaining two electrolytes. This points to a different mechanism of adsorption/desorption of species at the film–solution interface in that electrolyte, especially when compared to the plain 14.8 M H_3PO_4. This fact once again demonstrates the role of the acetic acid additive in modifying the properties of the oxide–electrolyte interface during transpassive dissolution.

Conclusions

The experimental and modelling work carried out in the present investigation demonstrate that the transpassive dissolution of model Fe–Cr alloys in electrolytes used for electropolishing and anodic levelling of such materials is basically a surface process. It comprises two parallel dissolution pathways, namely, oxidative dissolution of Cr as chromate and isovalent dissolution of the main element, Fe, mediated by an adsorption/surface complexation step involving a solution-originating species. As electropolishing abilities have already been reported by others [2] for at least one of the electrolyte mixtures studied (H_3PO_4/CH_3COOH 2:8) at near-ambient temperature, a general conclusion is that the relative importance of transport and surface kinetic steps in the overall electropolishing mechanism is to be reconsidered. In order to predict accurately both the steady-state and the transient behaviour of a steel in an electropolishing electrolyte mixture, it is particularly important to consider the surface kinetic steps of the dissolution of individual alloy constituents in addition to the transport of reactants/products in the bulk solution. In this connection, a combined electrochemical–microscopic investigation of the polishing abilities of a range of electrolytes towards industrial ferritic steels in H_3PO_4/CH_3COOH mixtures is underway and the results will be reported in the near future.

References

1. Landolt D (1987) Electrochim Acta 32:1
2. Singh VB, Upadhyay BN (1998) Corros Sci 40:705
3. Matlosz M, Magaino S, Landolt D (1993) J Electrochem Soc 140:1365
4. Matlosz M, Magaino S, Landolt D (1994) J Electrochem Soc 141:410
5. Matlosz M (1995) Electrochim Acta 40:393
6. Bojinov M, Tzvetkoff T (2003) J Phys Chem B 107:5101
7. Betova I, Bojinov M, Kinnunen P, Pohjanne P, Saario, T (2002) Electrochim Acta 47:3335
8. Bojinov M, Fabricius G, Laitinen T, Saario T (1998) J Electrochem Soc 145:2043
9. Bojinov M, Betova I, Fabricius G, Laitinen T, Raicheff R, Saario T (1999) Corros Sci 41:1557
10. Bojinov M, Fabricius G, Laitinen T, Saario T (1999) Electrochim Acta 44:4331
11. Bai L, Conway B (1991) J Electrochem Soc 138:2897
12. Datta M, Vercruysse D (1990) J Electrochem Soc 137:4017
13. Macdonald DD (1992) J Electrochem Soc 139:3434
14. Barcia OE, D'Elia E, Frateur I, Mattos OR, Pébère N, Tribollet B (2002) Electrochim Acta 47:2109
15. Bojinov M, Fabricius G, Kinnunen P, Laitinen T, Mäkelä K, Saario T, Sundholm G (2001) J Electroanal Chem 504:29
16. Heusler KE (1997) Corros Sci 39:1177